MINERALOGICAL MAGAZINE, SEPTEMBER 1983, VOL. 47, PP. 335-45

Crystal–liquid partition coefficients for pyroxene, spinels, and melilite, in slags

E. WEARING*

Department of Geology and Mineralogy, Oxford University, Parks Road, Oxford, OX1 3PR

ABSTRACT. The chemistry of spinels, plagioclase, and iron-rich, normally zoned pyroxene and melilite from some metallurgical slags has been investigated by electron microprobe analysis. Minor element partition coefficients, some of which are composition-dependent, have been calculated from the analytical data. The pyroxene/liquid partition coefficients range from 4.03 to 0.03 in the order Ti/Zr, Al, Mn, Zn, Ba, Sn, Na, reflecting increasing incompatibility. The spinel/liquid partition coefficients range from 40.89 to 0.02 but in the order Ti, Ni, Mg/Zn, Al, Mn, Cu, Sn, Zr. However, Sn becomes very compatible when the pyroxene and spinels crystallize in association with cassiterite. Melilite greatly discriminates against the incorporation of minor elements into its crystal structure. The crystallization of these phases produces residual liquids enriched in Na, Mn, Zn, Sn, Ba, W, and Pb.

METALLURGICAL slags, with a range in bulk chemical composition, sometimes crystallize to give phases that also occur in rocks. The present slags provide evidence for the behaviour of elements such as Cu, Ni, Sn, Ti, Zn, and Zr, in particular the crystal–liquid partition coefficients for pyroxene, spinels, and melilite. In this study, all chemical partitioning is expressed in terms of the partition coefficient, D, of the appropriate oxide (where D equals wt. % of oxide in crystals/wt. % of oxide in liquid).

Partition coefficients depend on pressure (1 atm. for slags), temperature (generally unknown for these slags), and bulk and trace element compositions, of both the melts and the crystals. This compositional dependence of partition coefficients is greater than pressure and temperature (Mysen and Virgo, 1980), and is studied here.

Analytical techniques. All the mineral analyses were made using a Cambridge Scientific Instruments Microscan 9 electron microprobe analyser. Computer corrections for ZAF effects were applied to all raw data. Spectrometer scans were used to detect the constituent elements for each phase. The bulk compositions (Table I) were determined by crushing large volumes of each slag and preparing a fused sample in a Pt crucible in air at 1300 °C. This glass was probed.

Mesostatic matrix, formed by the partial crystallization of residual liquid, is present in some of the slag samples. Such matrix compositions (Table II) were determined with the electron microprobe by analysing slightly devitrified glass (where the crystal size was no larger than 0.8 μm) over a wide area: a 100 μm raster was used instead of the usual 3 μm raster.

Chemistry and mineralogy of the samples

Tin slags. Eight of the slags came from tin reverberatory furnaces: their essentially CaO–Fe oxide–Al_2O_3–SiO_2 bulk compositions (see Table I) have significant amounts of SnO_2, ZrO_2, TiO_2, MnO, MgO, Na_2O, K_2O and ZnO. Two mineral assemblages have been recognized (and the constituent phases are listed in their order of crystallization): I. pyroxene/magnetite + melilite or plagioclase. II. melilite + magnetite + wüstite. Mesostatic matrix is present in both assemblages, although only the assemblage I matrix was suitable for analysis. Table I shows that the assemblage II samples are relatively CaO-richer and slightly SiO_2-poorer than the assemblage I samples.

Pyroxene. Pyroxene is present as phenocrysts in all the tin slags. The results of a step-scan from the core to the rim of a typical pyroxene crystal is shown in fig. 1 (see Table III for the representative pyroxene analyses). The most marked changes are in the increases in FeO and SiO_2, and decreases in Al_2O_3, MgO, and TiO_2. The concentrations of Na_2O, SnO_2, MnO, and ZnO are essentially constant, whereas CaO, ZrO_2, and BaO show slight decreases towards the rim. This pyroxene (see Table III) contains significant amounts of Al_2O_3, TiO_2, ZrO_2, SnO_2, and ZnO, and can be described as an aluminous hedenbergite. The Si deficiency in the tetrahedral (Z) sites of the clinopyroxene structure is assumed to be made up by Al. This Al_Z will be

* Present address: 210 Wingrove Road, Newcastle upon Tyne, NE4 9DD.

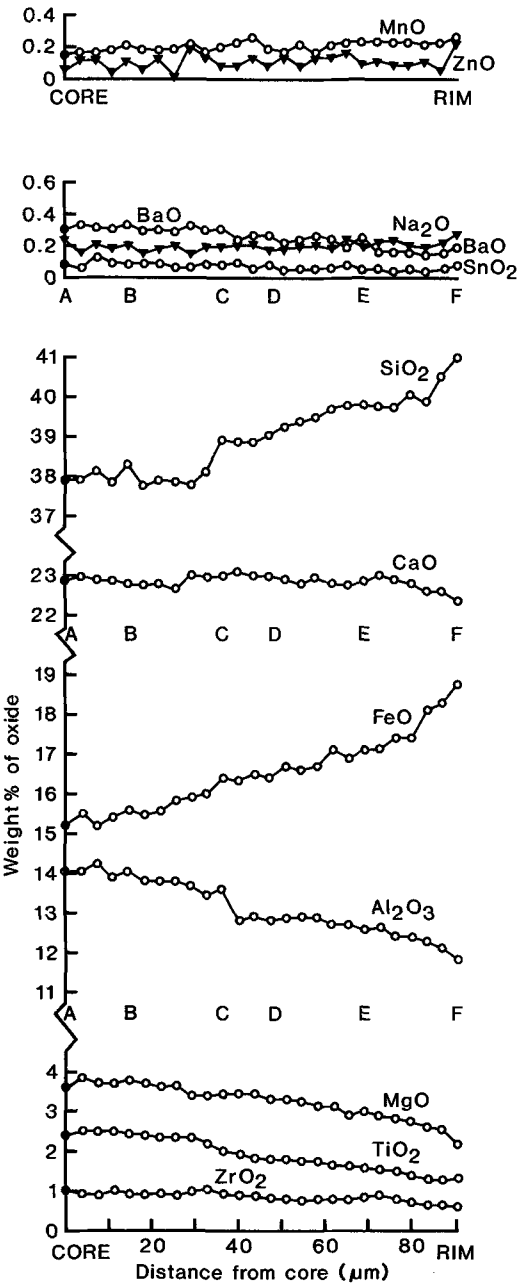

FIG. 1. Electron microprobe traverses across a typical pyroxene crystal from core to rim; letters A to F refer to representative analyses given in Table III.

partly balanced by the excess Al entering the octahedral (*Y*) sites as Ca-Tschermak. According to Verhoogen (1962) and Hartman (1969), Ti^{4+} is too large to enter *Z* and this must apply to the still larger Zr^{4+} and Sn^{4+}. The remaining Al_Z is probably balanced by the acceptance of Ti, Zr, and Sn into the octahedral sites.

Calculation of atomic ratios from the weight per cent analysis shows that the Al_Y remains constant at 0.21 to 0.19 cations (per formula unit of six oxygens) in both the core and rim. The Al zoning in fig. 1 is caused by Al_Z decreasing from 0.47 cations at the core to 0.35 at the rim. The substitution of Fe for Mg, with differentiation of the liquid, indicates a zoning pattern of increasing hedenbergite and decreasing diopside at approximately constant Ca-Tschermak.

Melilite. In assemblage I slags melilite is present as irregular prisms interstitial to the other phases, whereas the petrography of assemblage II slags is dominated by melilite phenocrysts. The melilite compositions (Table IV) are complex in relation to the commonly occurring end-members but can be described as containing significant amounts of ferro-akermanite (Fe-Ak), akermanite (Ak), soda-melilite (Nm) and gehlenite (Geh), with some hardystonite. Only the melilite in sample WH-26 was found to have significant compositional zoning. The zoning pattern, from core to rim, involves increasing Fe-Ak and Nm with decreasing Geh and Ak.

Wüstite (FeO). The melilite phenocrysts of assemblage II slags often contain microscopic rods of wüstite, which are orientated perpendicular to the faces of the host crystal. The beginning of wüstite crystallization coincides with the FeO enrichment of the melilite (WH-26), which must reflect iron enrichment of the residual liquid. Wearing (1982) considers that these rods, and their constant orientation, result from FeO saturation of the melt at the growth front of the melilite crystals.

Plagioclase. In sample WH-13 plagioclase has crystallized instead of the groundmass melilite, and is zoned from $An_{89}Ab_{11}$ to $An_{83}Ab_{17}$ (Table V).

Magnetite. Magnetite is included by all phases, and its compositions (Table VI) contain significant TiO_2 (up to 15.54 wt. %), Al_2O_3 (up to 12.45 wt. %), and ZnO (up to 1.03 wt. %), as well as minor amounts of CoO, CaO, and ZrO_2.

Cassiterite. When cassiterite is a crystallization product (sample WH-16), pyroxene and magnetite contain up to 7.84 wt. % and 5.30 wt. % SnO_2 respectively (see Tables III and VI).

There is little other data on similar slags, although Butler (1978) has described the mineralogy of a comparable tin slag, which crystallized garnet, pyroxene, melilite, spinel, and cassiterite. The garnet contained up to 26.26 wt. % SnO_2, whilst the pyroxene and magnetite contained 12.04 wt. % and 10.41 wt. % SnO_2 respectively. These tin

Table I. Bulk compositions of tin reverberatory slags

	Assemblage I						Assemblage II	
	WH-4	WH-7	WH-10	WH-13	WH-15	WH-16	WH-26	WH-33
SiO_2	30.56	33.43	33.36	33.19	33.08	31.66	29.98	31.06
Al_2O_3	10.62	10.43	10.20	11.11	11.10	10.75	8.49	9.83
TiO_2	2.36	1.73	1.59	2.99	2.75	2.69	1.81	1.64
Fe_2O_3	7.80	7.35	5.46	4.73	6.37	6.19	5.17	4.70
MgO	1.41	1.67	1.84	1.65	1.61	1.70	1.24	1.72
FeO	22.79	20.39	21.45	22.25	20.93	16.42	21.34	17.81
MnO	0.43	0.41	0.39	0.32	0.33	0.35	0.50	0.38
CaO	17.26	17.61	17.78	16.79	17.36	17.22	23.83	25.66
Na_2O	2.21	2.23	3.02	1.12	2.54	2.93	2.31	1.76
K_2O	0.52	0.51	0.64	0.89	0.62	0.60	0.50	0.46
SnO_2	0.36	0.43	0.88	0.08	0.34	5.75	1.98	1.55
ZnO	0.53	0.97	0.35	1.02	0.35	0.52	0.39	0.21
ZrO_2	0.34	0.35	0.35	0.46	0.49	0.46	0.39	0.34
BaO	0.29	0.39	0.33	0.22	0.28	0.30	0.42	0.27
WO_3	1.82	1.91	1.88	2.33	1.78	1.77	1.51	1.66
	99.30	99.81	99.52	99.26	99.93	99.31	99.86	99.03

(Fe_2O_3 has been calculated from the mineral compositions)

Table II. Residual liquid compositions of tin reverberatory slags

	Assemblage I					
	WH-4	WH-7	WH-10	WH-13	WH-15	WH-16
SiO_2	28.81	33.32	35.50	33.15	31.54	42.50
Al_2O_3	9.97	10.21	11.02	5.52	7.54	12.90
TiO_2	0.31	0.36	0.38	0.36	0.55	1.06
Fe_2O_3	n.d.	n.d.	n.d.	n.d.	n.d.	n.d.
MgO	0.30	0.52	0.58	0.24	0.41	0.23
FeO	19.86	22.86	26.93	26.99	28.97	7.96
MnO	0.44	0.43	0.57	0.45	0.57	0.31
CaO	19.38	17.74	12.44	18.02	18.96	18.48
Na_2O	6.04	5.36	5.77	3.15	4.24	3.74
K_2O	0.91	1.16	1.97	2.43	0.78	1.61
SnO_2	0.17	0.46	0.56	0.22	0.37	0.86
ZnO	0.27	0.60	0.27	0.82	0.46	0.41
ZrO_2	0.25	0.29	0.39	0.25	0.22	0.41
BaO	0.22	0.41	0.47	0.40	0.43	0.55
WO_3	11.66	5.14	3.03	6.40	5.25	4.37
CoO	0.08	0.06	0.05	0.06	0.06	0.06
PbO	0.06	0.05	0.05	0.06	0.05	0.03
	98.73	98.97	99.98	98.52	100.40	95.48

(n.d. = not determined)

Table III. Representative electron microprobe analyses for pyroxene step-scan shown in fig. 1, and a pyroxene analysis from sample WH-16.

	A	B	C	D	E	F	WH-16
SiO_2	37.93	38.31	38.87	39.04	39.06	40.99	33.65
Al_2O_3	14.02	14.02	13.58	12.84	12.58	11.77	12.06
TiO_2	2.42	2.43	2.01	1.77	1.58	1.34	3.04
MgO	3.67	3.78	3.45	3.33	2.99	2.14	4.49
FeO	15.22	15.61	16.41	16.43	17.09	18.74	15.42
MnO	0.16	0.22	0.20	0.19	0.23	0.27	0.21
CaO	22.94	22.79	23.00	23.03	22.78	22.34	22.46
Na_2O	0.23	0.20	0.20	0.18	0.20	0.28	0.60
ZnO	0.06	0.12	0.09	0.09	0.09	0.23	0.16
ZrO_2	0.99	0.93	0.90	0.80	0.83	0.61	0.56
BaO	0.30	0.34	0.32	0.27	0.25	0.20	0.13
SnO_2	0.09	0.08	0.09	0.09	0.05	0.08	7.84
	98.03	98.83	99.12	98.06	97.73	98.99	100.62
STRUCTURAL FORMULA BASED ON 6.0 OXYGENS							
Si	1.531	1.535	1.557	1.581	1.591	1.651	1.397
Al^{iv}	0.469	0.465	0.443	0.419	0.409	0.349	0.590
Al^{vi}	0.198	0.197	0.198	0.194	0.195	0.209	0.000
Ti	0.073	0.073	0.061	0.054	0.048	0.041	0.095
Mg	0.221	0.226	0.206	0.201	0.182	0.128	0.278
Fe^{2+}	0.514	0.523	0.550	0.556	0.582	0.631	0.535
Mn	0.005	0.007	0.007	0.007	0.008	0.009	0.007
Ca	0.992	0.978	0.987	0.999	0.994	0.964	0.999
Na	0.018	0.016	0.016	0.014	0.016	0.022	0.048
Zn	0.002	0.004	0.003	0.003	0.003	0.007	0.005
Zr	0.019	0.018	0.018	0.016	0.016	0.012	0.011
Ba	0.005	0.005	0.005	0.004	0.004	0.003	0.002
Sn	0.001	0.001	0.001	0.001	0.001	0.001	0.130
	4.048	4.048	4.051	4.049	4.049	4.027	4.096

Table IV. Electron microprobe analyses of melilite (where c = core and r = rim)

	WH-4	WH-10	$WH-26_c$	$WH-26_r$	$WH-33_c$	$WH-33_r$
SiO_2	40.82	40.91	36.80	40.33	36.39	37.15
Al_2O_3	8.92	8.47	12.06	8.48	13.32	11.94
TiO_2	0.04	0.04	0.06	0.00	0.06	0.06
MgO	1.09	2.85	2.53	1.23	2.83	2.99
FeO	12.27	9.24	9.09	12.62	8.63	9.01
MnO	0.12	0.14	0.14	0.22	0.12	0.12
CaO	31.07	33.02	35.82	32.44	36.05	35.98
Na_2O	4.56	3.65	2.00	3.49	1.83	1.89
K_2O	0.12	0.06	0.08	0.18	0.08	0.11
ZnO	1.07	0.64	0.32	0.25	0.32	0.27
ZrO_2	0.00	0.00	0.00	0.00	0.00	0.00
SnO_2	0.07	0.02	0.08	0.08	0.05	0.03
BaO	0.03	0.04	0.05	0.08	0.03	0.03
	100.18	99.08	99.03	99.40	99.71	99.58
STRUCTURAL FORMULA BASED ON 7.0 OXYGENS						
Si	1.925	1.929	1.750	1.924	1.713	1.754
Al	0.496	0.471	0.676	0.476	0.739	0.664
Ti	0.001	0.001	0.002	0.000	0.002	0.002
Mg	0.077	0.200	0.179	0.087	0.199	0.210
Fe	0.484	0.364	0.362	0.503	0.340	0.356
Mn	0.005	0.006	0.006	0.009	0.005	0.005
Ca	1.570	1.668	1.825	1.658	1.818	1.820
Na	0.417	0.334	0.184	0.323	0.167	0.173
K	0.007	0.004	0.005	0.011	0.005	0.007
Zn	0.037	0.022	0.011	0.009	0.011	0.009
Zr	0.000	0.000	0.000	0.000	0.000	0.000
Sn	0.001	0.000	0.002	0.002	0.001	0.001
Ba	0.001	0.001	0.001	0.001	0.001	0.001
	5.021	5.000	5.003	5.003	5.001	5.002

contents probably represent minimum values for the limit of ionic replacement of Sn^{4+} in the structure of these minerals.

Pyroxene–liquid relationships. The phase diagram produced by Huebner and Turnock (1980) for natural pyroxene quadrilateral compositions, and presented as a series of isothermal sections, is potentially useful for understanding pyroxene–liquid relationships during crystallization. The slag pyroxenes (Table III) plot within the augite field of this phase diagram. From the pyroxene zoning trend, and the knowledge of the augite + liquid tie

lines (fig. 10 of Huebner and Turnock, 1980), it would be expected that the liquid would become richer in Fe and only slightly depleted in Ca, relative to the coexisting clinopyroxene. Therefore, the residual liquids of tin slags would move towards Fe-enriched compositions, and the crystallization of the clinopyroxene would not force the liquid into the field of Ca-poor pyroxene. This interpretation is confirmed by the observed residual liquid compositions (Table II), and the absence of a Ca-poor pyroxene.

Comparison of the data in Tables I, II, and III suggests that crystallization of pyroxene will produce a liquid depleted in SiO_2, whereas the zoning pattern in fig. 1 suggests that the liquid becomes progressively more silicic. The crystallization of magnetite with the pyroxene will result in silica enrichment of the liquids; this would explain (i) the pyroxene zoning pattern, and (ii) the slight silica enrichment of the observed residual liquids.

Copper slags. Eleven copper converter slags were also examined, and these have essentially SnO_2–NiO–ZnO–Cu_2O–PbO–Fe oxide–SiO_2 bulk compositions. Three mineral assemblages have been recognized (and the constituent phases are listed in the order of crystallization): A. nickel-olivine + spinel + delafossite ($Cu_2O \cdot Fe_2O_3$) + cuprite + cassiterite + bunsenite. B. cassiterite/spinel + delafossite + cuprite. C. spinel + delafossite + cuprite. A detailed account of the mineralogy and petrography of these copper slags appears in Wearing (1981). Only the spinels of assemblages B and C are suitable for the calculation of partition coefficients. The spinel has a complex composition (10.94–33.89 wt. % NiO, 2.25–16.49 wt. % ZnO, 2.79–10.93 wt. % FeO, 0.76–2.03 wt. % CuO, 2.20–62.63 wt. % Fe_2O_3, and 1.93–44.84 wt. % SnO_2) which can be described as ranging from essentially Ni_2SnO_4 to $(Ni,Fe^{2+})Fe^{3+}_2O_4$.

Finally, Fe oxide–SiO_2-rich copper slags (samples CW-39 and 36), composed of fayalite phenocrysts (containing up to 10.32 wt. % ZnO) and spinel octahedra, have been examined.

Site occupancy

These slags can provide information about the site occupancies of Ti, Zr, Sn, Ba, Zn, and Ni in pyroxene, spinel, melilite, and plagioclase. The structural formulae of these minerals can be written in terms of *X* (eight co-ordinated, large cation), *Y* (octahedral, intermediate-size cation), *Z* (tetrahedral, small cation), and O (oxygen): pyroxene XYZ_2O_6; spinel Y_2ZO_4; melilite $X_2Z_3O_7$; and plagioclase XZ_4O_8.

Titanium. It is generally accepted that Ti^{4+} is only able to enter the *Y* sites in pyroxene and spinel. The failure of titanium to enter melilite and plagioclase can therefore be explained by the absence of *Y* sites in these two minerals.

Tin. Butler (1978) states that the absence of tin from melilite (*and plagioclase, this study*), especially when compared with the large amounts in garnet, pyroxene, and spinel, suggests that tin is only able to enter *Y* sites, which are not present in melilite (*and plagioclase, this study*).

Zirconium. The presence of zirconium in both pyroxene and spinel but its absence in melilite and plagioclase suggests that Zr^{4+} acts in the same way as Ti^{4+} and Sn^{4+}.

Barium. Ba primarily replaces K in the feldspar structure, but may also replace Ca and Na (Deer *et al.*, 1966). This suggests that Ba replaces Ca and Na in the *X* site of pyroxene.

Nickel. Ni^{2+} is known to have greater crystal-field stabilization energy (CFSE) in octahedral co-ordination than in tetrahedral co-ordination. Therefore, Ni^{2+} tends to form more stable octahedral compounds such as nickel-olivine and the spinel in copper converter slags.

Zinc. Zn^{2+}, having a full orbital of d-electrons, receives no CFSE in octahedral co-ordination. Zn^{2+} replaces Fe^{2+} in the tetrahedral sites of both melilite and spinel. This work suggests that Zn^{2+} does not enter the plagioclase structure. The presence of Zn^{2+} in both pyroxene and fayalite shows its ability to substitute for Fe^{2+} in the octahedral sites.

Partition coefficients

Two partition coefficients can be calculated: (1) Partition coefficients calculated between the core composition (of the initial mineral phase) and the bulk composition are taken to represent equilibrium values at the liquidus. (2) Many of the minerals are compositionally zoned, and where the minor elements have an almost constant concentration towards the rim (see fig. 1), this is taken to be the equilibrium value in the mineral whilst the mesostatic composition (Table II) is assumed to be the liquid.

Pyroxene

The calculated partition coefficients (Table VII) have been plotted against (*a*) concentration of the oxide in the melt, and (*b*) the concentration of the oxide end-member in the pyroxene. Also, the values for TiO_2, SnO_2, Al_2O_3, and ZrO_2 have been plotted against (*a*) concentration of Al_2O_3 in the liquid, and (*b*) the calculated activity of SiO_2 in the liquid as defined by equation 3 of Nielsen and Drake (1979). The resultant relationships will be described, although only the most important will be reproduced graphically.

Tables V and VI. Electron probe analyses of (left) plagioclase in sample WH-13 and (right) magnetite from tin reverberatory slags

	core	rim
SiO_2	45.34	47.60
Al_2O_3	32.77	32.11
TiO_2	0.06	0.06
MgO	0.11	0.06
FeO	1.14	0.71
MnO	0.03	0.03
CaO	18.10	16.46
Na_2O	1.05	1.80
K_2O	0.20	0.41
SnO_2	0.02	0.02
ZrO_2	0.00	0.00
BaO	0.12	0.31
	98.94	99.57
TO 8 OXYGENS		
Si	2.128	2.207
Al	1.813	1.755
Ti	0.002	0.002
Mg	0.008	0.004
Fe	0.045	0.027
Mn	0.001	0.001
Ca	0.910	0.818
Na	0.095	0.162
K	0.012	0.024
Sn	0.000	0.000
Zr	0.000	0.000
Ba	0.002	0.006
	5.016	5.006

	WH-7	WH-10	WH-15	WH-16	WH-26	WH-33
SiO_2	0.04	0.00	0.08	0.08	0.03	0.11
Al_2O_3	11.75	9.19	9.20	4.66	12.45	11.86
TiO_2	10.40	15.54	13.86	1.85	14.16	15.39
Fe_2O_3	34.77	28.03	31.25	53.91	25.33	23.75
MgO	1.41	1.12	1.56	2.30	0.58	0.64
FeO	39.05	43.98	41.47	30.29	44.07	44.87
MnO	0.42	0.45	0.41	0.56	0.68	0.65
CaO	0.19	0.16	0.39	0.16	0.33	0.68
ZnO	0.84	0.64	0.71	1.03	0.18	0.35
CeO	0.00	0.00	0.07	0.18	0.11	0.00
ZrO_2	0.05	0.09	0.05	0.01	0.15	0.22
SnO_2	0.20	0.06	0.15	5.43	0.66	0.64
	99.12	99.26	99.20	100.46	98.76	99.16
STRUCTURAL FORMULA BASED ON 4.0 OXYGENS						
Si	0.001	0.000	0.003	0.003	0.001	0.004
Al	0.495	0.391	0.391	0.206	0.526	0.500
Ti	0.280	0.422	0.375	0.052	0.382	0.414
Fe^{3+}	0.935	0.761	0.847	1.521	0.684	0.639
Mg	0.075	0.060	0.084	0.129	0.031	0.034
Fe^{2+}	1.167	1.327	1.249	0.950	1.322	1.342
Mn	0.013	0.014	0.013	0.018	0.021	0.020
Ca	0.007	0.006	0.015	0.006	0.013	0.026
Zn	0.022	0.017	0.019	0.029	0.005	0.009
Co	0.000	0.000	0.002	0.005	0.003	0.000
Zr	0.001	0.002	0.001	0.000	0.003	0.009
Sn	0.003	0.001	0.002	0.081	0.004	0.009
	3.000	3.000	3.000	3.000	3.000	3.000

The Fe_2O_3 concentration in magnetite was estimated by charge balancing the computed formula. This is accomplished by the equations (1) Fe^{3+} = ideal cation charge — actual cation charge
(2) Fe^{2+} = total Fe — Fe^{3+}
followed by altering the chemical analysis.

Table VII. Partition coefficients, calculated from tin slags, for pyroxene, magnetite, and melilite.

1. PYROXENE (c=core & r=rim)

Sample	ZnO	TiO_2	ZrO_2	SnO_2	Al_2O_3	MnO	Na_2O	BaO
$WH4_c$	0.21	0.98	3.00	1.08	1.33	0.30	0.09	0.21
$WH4_r$	0.89	3.90	3.08	2.18	1.20	0.55	0.03	0.18
$WH7_c$	0.06	1.40	2.83	0.21	1.34	0.39	0.10	0.77
$WH7_r$	0.38	3.72	2.10	0.20	1.15	0.63	0.05	0.49
$WH10_c$	0.23	1.69	2.60	0.52	1.33	0.46	0.08	n.d.
$WH10_r$	0.30	3.71	1.77	0.39	0.91	0.54	0.06	n.d.
$WH13_c$	0.57	1.09	2.17	0.38	1.02	0.47	0.14	0.55
$WH13_r$	0.65	4.03	3.80	0.32	1.23	0.78	0.06	0.15
$WH15_c$	0.49	1.03	2.20	0.56	1.20	0.67	0.12	n.d.
$WH15_r$	0.20	3.29	2.60	0.41	1.23	0.40	0.11	n.d.
$WH16_c$	0.44	0.93	1.09	0.87	1.05	0.66	0.25	0.30
$WH16_r$	0.85	3.08	1.37	3.67	0.82	1.26	0.23	0.22

(n.d. = not determined)

2. MAGNETITE

Sample	ZnO	TiO_2	ZrO_2	SnO_2	Al_2O_3	MgO	MnO
WH7	1.40	28.89	0.17	0.43	1.15	2.71	0.98
WH10	2.37	40.89	0.23	0.27	0.88	2.64	0.82
WH15	1.54	17.18	0.32	0.43	1.25	3.80	0.72
WH16	2.67	1.75	0.02	6.31	0.36	10.13	1.81
WH22	n.d.	4.73	0.10	0.14	0.25	12.00	n.d.

3. MELILITE

Sample	MgO	FeO	Al_2O_3	Na_2O	ZnO	MnO	K_2O	BaO
WH4	3.63	0.62	0.89	0.75	3.96	0.27	0.13	0.04
WH10	4.91	0.34	0.77	0.63	2.37	0.25	0.03	0.08
WH26	2.04	0.43	1.42	0.86	0.82	0.28	0.16	0.12
WH33	1.65	0.48	1.36	1.04	1.52	0.32	0.17	0.11

4. PLAGIOCLASE : see text

Table VIII. Experimentally-determined partition coefficients for comparison with the values listed in Table I.

1. AUGITE

a. Duke (1976): MnO 0.55-0.75
TiO_2 0.23-0.55

b. Biggar et al (1971): MnO 0.97-1.20
TiO_2 0.28-0.31
Al_2O_3 0.31-0.37

c. Huebner and Turnock (1980): MnO 0.34-1.25 (average 0.67)
TiO_2 0.14-0.26 (average 0.20)
Al_2O_3 0.10-0.20 (average 0.14)

d. O'Hara et al (1974) :

	1108°C	1120°C	1130°C
Na_2O	0.15	0.22	0.16
TiO_2	0.37	0.55	0.33
Al_2O_3	0.26	0.49	0.28

2. PLAGIOCLASE

O'Hara et al (1974) :

	1108°C	1120°C	1130°C
TiO_2	0.05	0.02	0.03
Al_2O_3	3.13	3.59	3.47
FeO	0.05	0.04	0.05
MgO	0.05	0.03	0.05
Na_2O	2.15	1.71	1.79
	An_{85}	An_{93}	An_{93}

Table IX. Partition coefficients, calculated from copper slags, for spinel and fayalite.

1. SPINEL

Sample	TiO_2	Al_2O_3	MgO	ZnO	SnO_2	NiO
assemblage A						
CW1	1.2	0.9	1.4	1.8	2.1	2.1
CW2	2.5	0.9	1.4	1.8	2.2	2.2
CW5	2.5	1.4	1.8	1.9	1.8	1.7
CW23	3.0	0.8	1.5	1.0	1.7	1.7
CW33	3.0	1.1	2.4	2.0	2.3	2.3
CW34	2.5	1.1	1.7	1.8	2.0	2.1
assemblage B						
CW4	2.5	2.4	1.8	1.9	1.6	1.9
CW8	2.0	1.3	1.7	2.9	0.6	4.0
CW20	1.1	1.5	1.4	2.3	1.0	3.8
CW21	1.6	1.0	2.2	0.9	2.8	3.4
CW29	1.6	1.4	1.7	1.7	1.2	1.8
Fe oxide-SiO_2 —rich copper slags						
CW36	2.8	1.3	3.8	1.2	2.0	–
CW39	25.8	0.5	1.6	1.3	0.6	–

2. FAYALITE

	TiO_2	Al_2O_3	MgO	ZnO	CaO	CuO
CW39	0.01	0.30	3.70	2.90	0.03	0.07

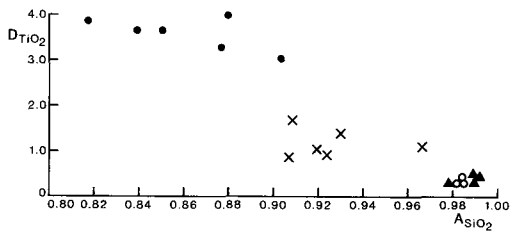

FIG. 2. The TiO_2 partition coefficients for pyroxene plotted against the calculated SiO_2 activity (A_{SiO_2}) in the liquid. Crosses represent core determinations whilst solid circles represent rim determinations; the solid triangles show values from O'Hara *et al.* (1974) and the open circles those from Biggar *et al.* (1971).

TiO_2. Plotting D_{TiO_2} against the calculated activity of SiO_2 (fig. 2), shows a rough relation of increasing D_{TiO_2} as SiO_2 activity decreases. Akella and Boyd (1973) found that the addition of SiO_2 to their systems decreased D_{TiO_2} for pyroxene. Fig. 3 shows that D_{TiO_2} is inversely related to the concentration of TiO_2 in the melt. However, D_{TiO_2} shows no relationship to either the concentration of Al_2O_3 in the melt or the mol. % of Ti-pyroxene.

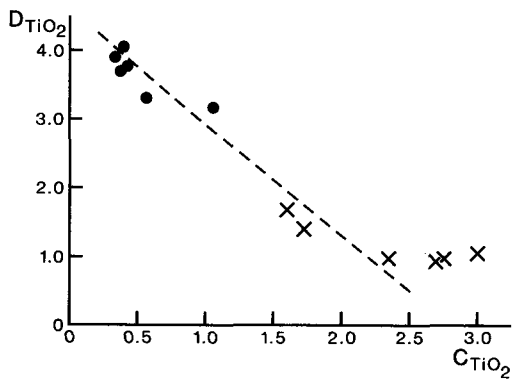

FIG. 3. The TiO_2 partition coefficients for pyroxene plotted against the TiO_2 concentrations in the liquid (C_{TiO_2}). Crosses represent core determinations whilst solid circles represent rim determinations.

The involvement of TiO_2 in the pyroxene zoning implies disequilibrium and therefore, the D_{TiO_2} values will be similarly in disequilibrium. At the same time the TiO_2 is being continually depleted from the melt by the crystallization of magnetite and pyroxene. Thus, the variation in D_{TiO_2} with melt composition may be a disequilibrium feature. As for the variation of D_{TiO_2} with temperature (not studied here), Duke (1976) found that D_{TiO_2} for clinopyroxene has no systematic variation with temperature.

SnO_2. D_{SnO_2} shows no relationship to any variable. However, only the pyroxene rim of WH-16, which produced the highest D_{SnO_2} value (3.67) in Table VII, has crystallized in association with cassiterite. When cassiterite is crystallizing the SnO_2 activity of the liquid is 1, but in the absence of cassiterite will be less than 1. Thus, the D_{SnO_2} will be higher for a SnO_2 activity in the liquid of 1 than for a SnO_2 activity less than 1.

ZrO_2. D_{ZrO_2} is not related to the activity of SiO_2, the Al_2O_3 concentration of the melt, or the mol. % of Zr-pyroxene, but shows an inverse correlation with the concentration of ZrO_2 in the melt (fig. 4). The rim and core values plot together to define the same trend, suggesting that this is definitely not a disequilibrium feature.

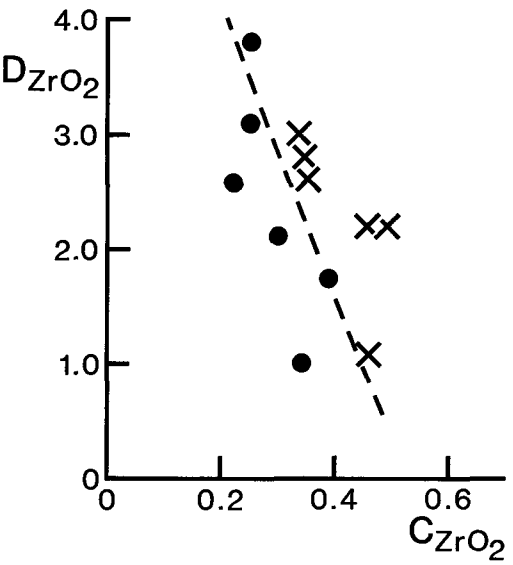

FIG. 4. The ZrO_2 partition coefficients for pyroxene plotted against the ZrO_2 concentrations in the liquid (C_{ZrO_2}). Crosses represent core determinations whilst solid circles represent rim determinations.

Al_2O_3. $D_{Al_2O_3}$ shows no relationship to any variable. However, the crystallization of Al-rich phases such as melilite and plagioclase will control the availability of Al_2O_3 in the liquid for substitution into pyroxene.

$R^{2+}O$. Plotting D_{ZnO}, D_{BaO}, and D_{MnO} against their respective oxide concentrations in the liquid produces a scattered pattern. However, these oxides would be expected to obey Henry's Law (see Wood and Fraser, 1976) which would produce a constant value of D at varying concentrations in the melt. These observed patterns suggest either disequilibrium or error. Disequilibrium could be

caused by either the influence of other minerals or the balance between crystal growth and chemical gradients.

When D_{MnO} and D_{ZnO} are plotted respectively against mol. % Mn-pyroxene and mol. % Zn-pyroxene (fig. 5), there is a distinct correlation.

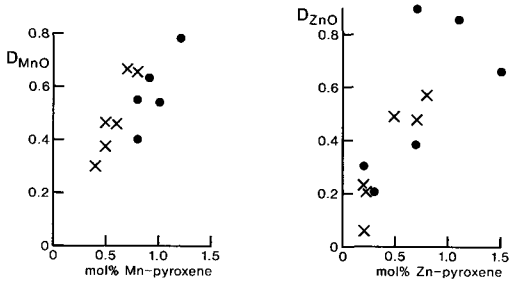

FIG. 5. The MnO and ZnO partition coefficients for pyroxene plotted respectively against the concentration of their oxide end-members in the pyroxene. Crosses represent core determinations whilst solid circles represent rim determinations.

Therefore, these two partition coefficients are related to the composition of the pyroxene (i.e. the availability of sites into which Mn and Zn can substitute). The similarity of core and rim compositions in different samples suggests the absence of temperature control. Duke (1976) found that D_{MnO} for clinopyroxene varies systematically with temperature but considers that the range is not extreme and so may be due to the Mg/Fe ratio of the mineral.

Na_2O. D_{Na_2O} appears to be controlled by the concentration of Na_2O in the melt. However, the concentration of Na_2O in the solid is approximately constant whilst it is continually concentrated in the residual liquid.

Discussion. There are no experimentally determined values of D for ferrohedenbergite in the literature, although the available data for augite (Table VIII) can be used for a comparative study. These experimental data found the D values to be independent of consistent temperature and compositional controls.

The $D_{Al_2O_3}$ values of these slags (0.82–1.34) are significantly greater than those determined experimentally. When the values of Biggar *et al.* (1971) and O'Hara *et al.* (1974) are added to the $D_{Al_2O_3}$–a_{SiO_2} plot (fig. 6), this difference may be explained by the experimental values coming from liquids with a higher SiO_2 activity than these slags. The concentration of Al_2O_3 in the experimental liquid is similar to that of the liquid slag and therefore, $D_{Al_2O_3}$ is unrelated to the Al_2O_3 content of the liquid but possibly to the a_{SiO_2}.

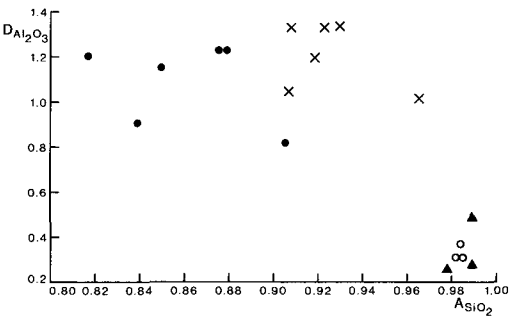

FIG. 6. The Al_2O_3 partition coefficients, for pyroxene, plotted against the calculated SiO_2 activity (A_{SiO_2}) in the liquid. Crosses represent core determinations whilst solid circles represent rim determinations; the solid triangles show values from O'Hara *et al.* (1974) and the open circles those from Biggar *et al.* (1971).

The experimentally determined values of D_{TiO_2} (0.14–0.55) are less than 1, whilst those values for slags are greater than 1. The experimental melt compositions of Huebner and Turnock (1980) were similar to the TiO_2 content of the slags (0.31–2.99 wt. %), but those of the other studies had up to 10.46 wt. % TiO_2. This suggests that D_{TiO_2} may be independent of the TiO_2 content of the melt. When the values of Biggar *et al.* (1971) and O'Hara *et al.* (1974) are added to the D_{TiO_2}–a_{SiO_2} plot (fig. 2) they fall approximately on the trend defined by the slag values. Thus, whether D_{TiO_2} is incompatible or compatible appears to be controlled by the SiO_2 activity of the liquid.

The D_{MnO} values calculated from the slags (0.30–1.26) compare favourably with those determined experimentally (0.34–1.25). Similarly, the D_{Na_2O} values of slags (0.03–0.25) are similar to those given by O'Hara *et al.*, 1974 (0.15–0.22). Unfortunately, the other oxide D values have no comparable data. The apparent good fit of D_{Na_2O} and D_{MnO} with the experimental data, suggests that the calculated D_{ZnO}, D_{BaO}, D_{ZrO_2}, and D_{SnO_2} may be similar to those of natural systems.

Magnetite

Only those magnetite crystals within the mesostatic matrix were suitable for electron microprobe analysis. Subsequently, there is a limited number of calculated D values to determine correlations with possible variables. The D values (Table VII) have been plotted against (*a*) the concentration of the oxide in the melt, and (*b*) the concentration of the oxide end-member in the spinel. Oxygen fugacity cannot be plotted as a variable.

TiO_2. D_{TiO_2} shows rough inverse correlation with the TiO_2 content of the liquid, and possibly with the mol. % ulvöspinel of the spinel (fig. 7). However, the

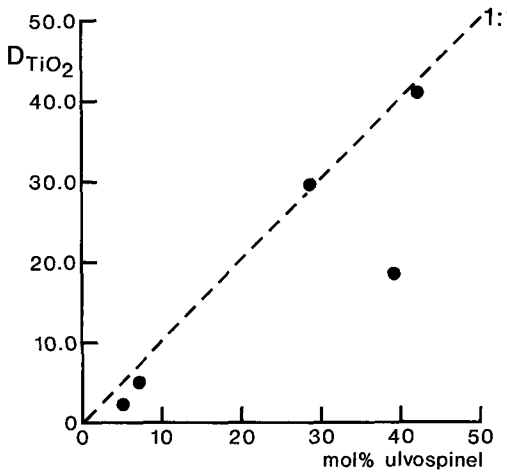

FIG. 7. The TiO_2 partition coefficients for magnetite plotted against the concentration of ulvöspinel in the magnetite.

content of the ulvöspinel molecule is dependent on temperature, so that D_{TiO_2} depends also on the temperature.

SnO_2. D_{SnO_2} may be related to the mol. % Sn-spinel (fig. 8) in a similar way to that described for D_{TiO_2} and the mol. % ulvospinel. In those samples not crystallizing cassiterite, D_{SnO_2} is between 0.14 and 0.43. However, in WH16 D_{SnO_2} is 6.31 which corresponds to the presence of cassiterite; in such liquids the SnO_2 activity will be 1, which will enable a higher value of D than liquids lacking cassiterite where SnO_2 activity will be less than 1.

Al_2O_3. $D_{Al_2O_3}$ shows a possible correlation with the Al_2O_3 content of the liquid, but is independent of spinel composition.

ZrO_2. D_{ZrO_2} has no distinct correlations with the variables, and the contents involved are small in concentration.

$R^{2+}O$. Plotting D_{ZnO}, D_{MgO}, and D_{MnO} against the two variables, there are no distinct correlations.

CuO. D_{CuO} values of 0.4 and 0.7 have been calculated from two samples of Fe oxide-SiO_2-rich copper slag.

Discussion. Magnetites from igneous rocks have wide variations in composition because of variations in the composition, temperature, and oxygen fugacity of the host liquid. Despite this, there is little published data on magnetite/liquid partition coefficients. Leeman *et al.* (1978) calculated an average D_{TiO_2} value of 25.0 ($\pm$8.0) for ideal Rayleigh (i.e. fractional) crystallization, and an average value of 34.0 ($\pm$6.0) for ideal Nernst (i.e. equilibrium) crystallization. However, because these values were obtained from crystallization models, with incorporated uncertainties, the authors consider the accuracy of their estimated values to be no better than $\pm$25%.

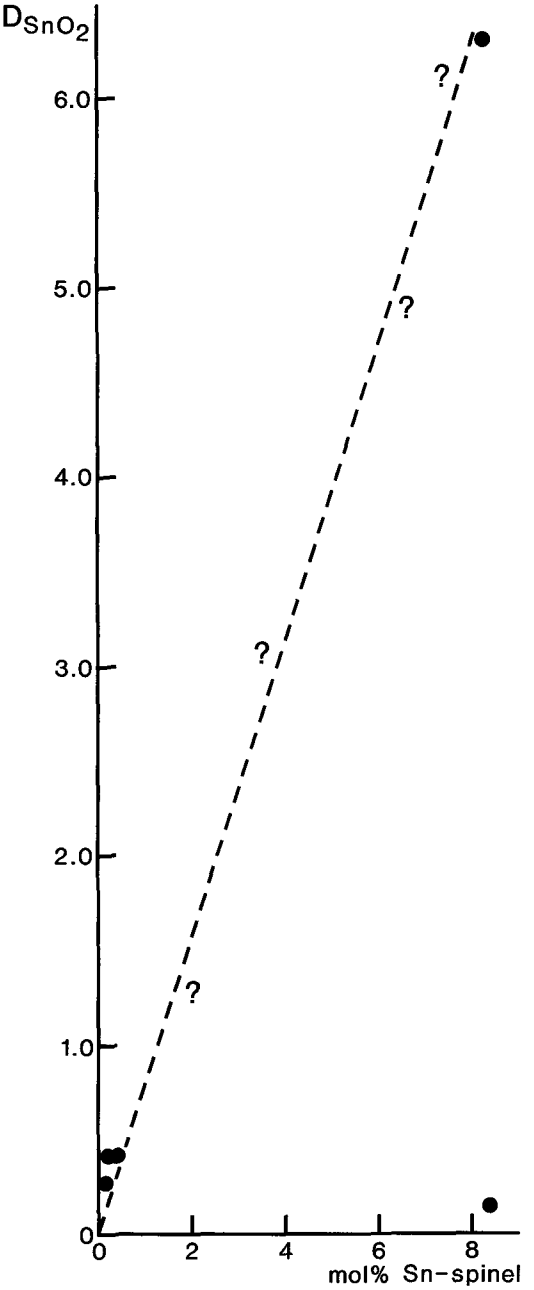

FIG. 8. The SnO_2 partition coefficients for magnetite plotted against the concentration of Sn-spinel in the magnetite.

The crystallization of tin slags will approach the

Rayleigh model. Excluding the cassiterite-bearing sample, D_{TiO_2} values are between 17.18 and 40.89. The two sets of values calculated by Leeman *et al.* (1978) fall within this range, suggesting that D_{TiO_2} values cannot be used to determine the type of crystallization.

Spinel from the copper converter slags

The calculated partition coefficients (Table IX) have been plotted against (*a*) the concentration of the oxide in the melt, and (*b*) the concentration of the oxide (as cations) in the spinel. Cations were used instead of end-members because of the complex compositions.

ZnO and MgO. Plotting D_{ZnO} and D_{MgO} against their respective oxide concentrations in the liquid produces a scattered pattern.

TiO_2 and Al_2O_3. D_{TiO_2} and $D_{Al_2O_3}$ are unrelated to the two variables.

SnO_2. D_{SnO_2} cannot be correlated with any variables. However, the values for the assemblage A spinels are higher than for the assemblage B spinels. This can be explained by the early crystallization of cassiterite in the assemblage A slags (i.e. the SnO_2 activity of the liquid is 1) but by its absence in the assemblage B slags (where the SnO_2 activity will be less than 1).

NiO. D_{NiO} is inversely related to both the NiO concentrations of the liquid and the composition of the spinel (fig. 9), but there are no obvious reasons to explain these correlations. However, when D_{NiO} is plotted against the concentration of ZnO and FeO of the liquid (fig. 10), there are inverse correlations. Thus, D_{NiO} decreases as the ZnO and

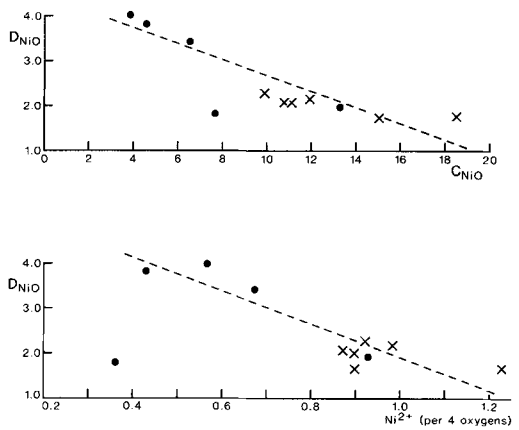

FIG. 9. The NiO partition coefficients for (copper converter slag) spinel plotted against (*a*) the concentration of NiO in the liquid (C_{NiO}), and (*b*) the Ni^{2+} cations (per four oxygens) in the spinel compositions. The crosses represent assemblage A spinels and the solid circles represent assemblage B spinels.

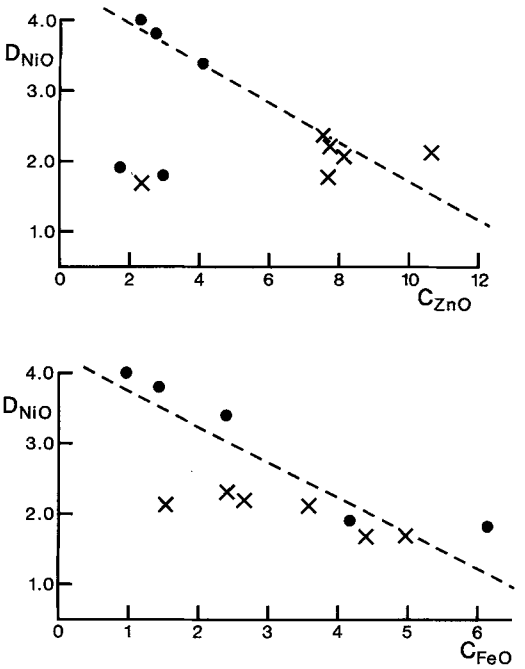

FIG. 10. The NiO partition coefficients for (copper converter slag) spinel plotted against the concentration of (*a*) ZnO in the liquid (C_{ZnO}), and (*b*) FeO in the liquid (C_{FeO}). The crosses represent assemblage A spinels and the solid circles represent assemblage B spinels.

FeO of the liquid increases. In comparison, there is no correlation between D_{ZnO} and concentration of NiO in the liquid. This suggests that the D_{NiO} is controlled by the $R^{2+}O$ content of the liquid.

Fayalite

Partition coefficients have been calculated between fayalite and residual liquid (Table IX) in copper slag CW-39. These values range from 3.70 to 0.01 in the order Mg, Zn, Al, Cu, Ca, Ti, reflecting increasing incompatibility.

Melilite

The restricted number of calculated *D* for melilite (Table VII) prevents any attempt to investigate the possible controls. Furthermore, the oxides MgO, FeO, Al_2O_3, Na_2O, and ZnO are involved in zoning, so that the partition coefficients will be continually changing their values. Samples WH-26 and -33 provide core–bulk composition determinations, which probably approach equilibrium values for those compositions. No experimentally determined *D* values for melilite appear in the literature.

Plagioclase

In sample WH-13, D values have been calculated between the plagioclase rim and the mesostatic matrix: $D_{K_2O} = 0.2$, $D_{BaO} = 0.4$, and $D_{FeO} = 0.03$. The D_{FeO} value compares favourably with those given by O'Hara *et al.*, 1974 (Table VIII). Values of D_{K_2O} and D_{BaO} in basalts are given by Cox *et al.* (1979). The calculated D_{K_2O} is similar whilst the difference of D_{BaO} is probably within electron microprobe error because of its low concentration.

Effect of liquid composition

The partition coefficient data studied above indicate that the D_{MnO}, D_{ZnO}, and D_{BaO} values are independent of liquid composition. The D_{SnO_2} values are independent of liquid composition, although they are related to the SnO_2 activity in the liquid (i.e. whether cassiterite is present or not). In comparison, $D_{Al_2O_3}$, D_{TiO_2}, and D_{ZrO_2} are dependent on the melt composition.

Compatibility/incompatibility of the elements

Pyroxene. The D values range from 4.03 to 0.03 (Table VII) in the order Ti/Zr, Al, Mn, Zn, Ba, Sn, Na, reflecting increasing incompatibility. At the pyroxene cores Ti is less compatible than Zr, but the relationship is reversed at the rims. This change in compatibility is probably a result of the change in the ratio of these elements in the liquid.

Na is the most incompatible element which is able to enter pyroxene. The other four incompatible elements have no constant relationship to each other. This is because D_{MnO} and D_{ZnO} are related to the site availability in the pyroxene. Therefore, these incompatible elements will be enriched in the residual liquids to different amounts.

Magnetite (tin slags). The D values range from 40.89 to 0.02 (Table VII) in the order Ti, Mg, Zn, Al, Mn, Cu, Sn, Zr, reflecting increasing incompatibility.

Opaque spinel (copper slags). The D values calculated from the assemblage B slags (Table IX) range from 4.0 to 0.6, although D_{TiO_2} fluctuates because of the small concentrations involved. The order of decreasing compatibility sometimes varies, although is typically Ni, Zn, Mg, Al, Sn. The D values calculated from the assemblage A slags range from 3.0 to 0.8 in the order Ni/Sn, Zn, Mg, Al, reflecting decreasing compatibility. The change in the role of Sn, relative to assemblage B, is due to the crystallization of cassiterite.

By combining the spinel/liquid partition coefficient data from tin and copper slags, the order of increasing incompatibility is either (i) cassiterite absent: Ti, Ni, Mg/Zn, Al, Mn, Cu, Sn, Zr or (ii) cassiterite present: Sn, Ni, Ti, Mg/Zn, Al, Mn, Cu, Zr.

Minor oxide behaviour during crystallization

From these partition coefficient data, combined with the known site occupancies in each mineral, proposals can be made for the behaviour of each minor oxide during the crystallization of tin slags.

TiO_2 and Al_2O_3. The preference of TiO_2 to enter magnetite instead of pyroxene in the cassiterite-free assemblage I tin slags, has led to a strong TiO_2 depletion of the residual liquid. The TiO_2-rich character of these pyroxenes has been shown to reflect the increasing tendency for Ti to enter pyroxene in silica undersaturated systems. No firm conclusions can be drawn as to the role of $D^{px}_{Al_2O_3}$, since the amount of available Al_2O_3 will be controlled by the crystallization of other Al-rich minerals.

The inability of Ti to enter melilite will lead to TiO_2 enrichment in the residual liquids of assemblage II tin slags. The later crystallization of magnetite will remove some of this TiO_2, and so has probably prevented the formation of a Ti-rich mineral.

ZrO_2. Zirconium is unable to enter melilite and plagioclase, and only enters magnetite to a limited extent. This causes ZrO_2 enrichment in the residual liquids of assemblage II samples. In comparison, Zr is preferentially concentrated in the calcic pyroxenes, although no significant reasons can be found to explain this phenomena. This will lead to the depletion of ZrO_2 during the crystallization of assemblage I slags.

In igneous rocks ZrO_2 usually crystallizes out as late-stage zircon. However, the undersaturated character of the liquid slag will preclude the crystallization of zircon, so that the Zr is only able to leave the liquid by entering pyroxene. In natural liquids ZrO_2 only reaches significant concentrations in oversaturated compositions, where Zr is incompatible to the crystallizing pyroxene. This evidence would seem to suggest that $D^{px}_{ZrO_2}$ is in some way related to the activity of SiO_2 in the liquid. Because of the absence of $D^{px}_{ZrO_2}$ values from rocks, the compositional dependence of this partition coefficient cannot be verified for natural liquids.

SnO_2. In the absence of cassiterite, Sn is incompatible in pyroxene and magnetite, and is unable to enter the structures of plagioclase and melilite. Therefore, SnO_2 will become enriched in the residual liquids. The degree of enrichment will be greatest when melilite is the main phase, as in assemblage II samples. The petrography of sample WH-16 suggests that SnO_2 as cassiterite crystallized as a primary phase, because of the enrichment of tin in the residual liquid.

ZnO. Zinc is compatible in magnetite, melilite,

and olivine, and incompatible in pyroxene, but has difficulty in entering plagioclase. Therefore, depending on the crystalline phases ZnO will be either enriched or depleted in the residual liquids of slags. The enrichment will be greatest in slags which do not contain olivine.

NiO. Nickel is extremely compatible in spinel and olivine of copper converter slags, so that NiO will be depleted from the residual liquid.

MnO. Mn is incompatible in plagioclase, melilite, and pyroxene, and close to unity in magnetite, so that MnO will be enriched in the residual liquid.

BaO. Because of the size and charge of Ba^{2+}, it has difficulty in entering the structure of many minerals. When Ba is able to enter minerals, it is very incompatible and so is enriched in the residual liquid.

WO_3. Tungsten is present in tin slags but is unable to enter any mineral structures, and so becomes enriched in the residual liquid.

PbO. Lead is present in copper slags but it is wholly incompatible with the mineral phases. This results in the continual enrichment of PbO in the residual liquid.

CuO. The evidence for the role of CuO during crystallization is unclear from the slag samples. However, from the D_{CuO} values for spinel, it would be expected to be concentrated during crystallization.

Therefore, Na_2O, MnO, ZnO, SnO_2, BaO, WO_3, and PbO will become enriched in the residual liquids of tin slags.

Acknowledgements. The samples were provided by IMI Refiners Limited and Williams, Harvey and Co. Limited; the author gratefully acknowledges their permission to publish this paper. The technical assistance of Dr N. Charnley, Messrs C. R. Fagg, C. Johnson, K. A. Parrish, M. Slater, S. Wyatt, and the late R. A. Holland is particularly acknowleged. This work was supported by the NERC and supervised by Dr B. C. M. Butler.

REFERENCES

Akella, J., and Boyd, F. R. (1973) *Proc. Fourth Lunar Sci. Conf., Geochim. Cosmochim. Acta* (*Suppl.* **4**), 1049–59.

Biggar, G. M., O'Hara, M. J., Peckett, A., and Humphries, D. J. (1971) *Proc. Second Lunar Sci. Conf., Geochim. Cosmochim. Acta* (*Suppl.* **2**), 617–43.

Butler, B. C. M. (1978) *Mineral. Mag.* **42,** 487–92.

Cox, K. G., Bell, J. D., and Pankhurst, R. J. (1979) *The interpretation of igneous rocks.* George Allen & Unwin.

Deer, W. A., Howie, R. A., and Zussman, J. (1966). *An introduction to the rock-forming minerals.* Longman.

Duke, J. M. (1976) *J. Petrol.* **17,** 499–521.

Hartman, P. (1969) *Mineral. Mag.* **37,** 366–9.

Huebner, J. S., and Turnock, A. C. (1980) *Am Mineral.* **65,** 225–71.

Leeman, W. P., Ma, M.-S., Murali, A. V., and Schmitt, R. A. (1978) *Contrib. Mineral. Petrol.* **65,** 269–72.

Mysen, B. O., and Virgo, D. (1980) *Geochim. Cosmochim. Acta,* **44,** 1917–30.

Nielsen, R. L., and Drake, M. J. (1979) *Ibid.* **43,** 1259–72.

O'Hara, M. J., Biggar, G. M., Hill, P. G., Jefferies, B., and Humphries, D. J. (1974) *Earth. Planet. Sci. Lett.* **21,** 253–68.

Verhoogen, J. (1962) *Am. J. Sci.* **260,** 211–20.

Wearing, E. (1981) Unpub. D.Phil. thesis, University of Oxford.

——(1982) *Mineral. Mag.* **46,** 441–4.

Wood, B. J., and Fraser, D. G. (1976) *Elementary thermodynamics for geologists.* Oxford University Press.

[*Manuscript received 21 May 1982; revised 30 November 1982*]